Acta Acustica 2022, **6**, 27

https://doi.org/10.1051/aacus/2022022

Topical Issue - Aeroacoustics: state of art and future trends

Available online at:
https://acta-acustica.edpsciences.org

SCIENTIFIC ARTICLE OPEN ACCESS

Shielding of rotor noise by plates and wings

Michael Carley*

Department of Mechanical Engineering, University of Bath, Bath BA2 7AY, United Kingdom

Received 28 February 2022, Accepted 8 June 2022

Abstract – A method of noise reduction proposed for the next generation of aircraft is to shield noise from the propulsion system, by positioning the noise source over a wing or another surface. In this paper, an approximate analysis is developed for the acoustic field far from a circular source placed near the edge of a semi-infinite plate, a model problem for shielding of noise by a wing and for scattering by a trailing edge. The approximation is developed for a source of small radius and is found to be accurate when compared to full numerical evaluation of the field.

Keywords: Noise shielding, Rotor noise, Trailing edge, Scattering

1 Introduction

The effect of airframe configurations on the propagation of noise from propulsion systems is a question which has been studied over a number of years. In particular, studies have been conducted of the possibility of positioning propulsion systems in such a way that the airframe acts to "shield" the noise source and reduce noise levels reaching the ground. One example is the "Silent Aircraft" Initiative, in which a study was conducted of the scattering of noise from sources placed above the blended wing body configuration [1]. Another study [2] examined the effect of propeller positioning on an otherwise conventional airframe, making use of the tailplane for acoustic shielding. As electric propulsion improves, and novel configurations using airframe shielding for noise reduction become more feasible, there is a greater need for reliable methods which can be used in design and to provide insight into the propagation of sound around airframes.

The literature on the use of aircraft configurations to shield noise from propulsion systems is not as extensive as that on the reduction of noise at source, and has tended to concentrate on reducing environmental noise from jet and turbofan systems. Czech and Thomas [3] note that there have been very few studies on the installation effect on open rotors of airframe elements other than pylons. They report experimental studies of noise from an open rotor system on a conventional and on a hybrid wing body airframe, as part of an extensive study on installation and shielding effects [4–6]. The airframe configuration used in these tests had a swept trailing edge and so was not comparable to the model problem considered in this paper, but it did demonstrate shielding effects of up to 12 dB for certain axial displacements of the rotor [3].

The prediction of shielding effects on propulsion noise appears to have been carried out mainly using numerical approaches such as the use of computational fluid dynamics (CFD) data in a permeable surface integration method [7] or a boundary element method (BEM) calculation using a suitable model for the rotor source [8]. A comparison of shielding patterns from BEM predictions and experimental data has also shown good agreement in the case of a monopole point source [9] and gives confidence that the BEM is a suitable method for assessment of shielding when sufficient information about the aircraft configuration is available.

There does not appear to be a reliable method in the literature for approximate prediction of shielding effects. In a study of shielding of noise from a counter-rotation open rotor [10], two theories for shielding attenuation, barrier theory and half-plane diffraction, were compared to experimental data, approximating the rotor by a point source. It was found that neither gave accurate results, over-predicting the attenuation by 5 dB when the point source approximation was used. The error may have been increased by the source having a higher frequency than was used in developing the curve fits used in the barrier theory approximations [11].

The theory for shielding by a wing is based on the problem of diffraction by a semi-infinite plane, first addressed more than a century ago [12]. A comprehensive review of the theory of noise shielding [13] discusses in some depth the analysis of noise from point sources near shielding bodies and the different approximations which apply throughout the field. In particular, the applicability and breakdown of the geometric acoustics approximation is considered, as well as the existence of "shadow" zones around a shielding body, regions in which the source is not "visible", being blocked by the body. In this paper, the theory to be applied

*Corresponding author: m.j.carley@bath.ac.uk

will be the standard analysis of scattering by a semi-infinite plate, extended to include the effects of a mean flow [14].

The motivation for the work in this paper is then the lack of a reliable model for shielding of noise from rotating sources in aeronautical applications. We present an analysis of far-field noise from a rotating source which replaces the point source approximation with the models normally used in established theory for noise from rotating sources. The result is an approximation which compares well to full numerical solution and should be useful to designers and researchers as a starting point for parametric studies of rotor positioning in new configurations.

2 Analysis

The problem of scattering by a plane is an old one [12, 13], which has been extended to include the effect of mean flow in the acoustic case [14]. We begin by presenting existing results for the problem in a form which are then incorporated into standard methods for the calculation of the acoustic far field of rotating sources.

2.1 Green's function

The coordinate system used to analyze the scattering of sound by a semi-infinite plate is shown in Figure 1. A uniform flow of Mach number M_0 is imposed normal to the trailing edge. A Cartesian coordinate system (x, y, z) is centred on the edge of the plate, with x parallel to the flow, y normal to the plate and z aligned with the edge. A cylindrical coordinate system (r, θ, z) is defined, with $r = \sqrt{x^2 + y^2}$ and $\theta = \tan^{-1} y/x$. The Green's function for the field at a point (x, y, z) due to a source of time dependence $\exp[-i\omega t]$ at (x_0, y_0, z_0) is given by [14],

$$G(\mathbf{x}, \mathbf{x}_0) = \frac{e^{-iKM_0(X-X_0)}}{\beta}\left[g_1(\mathbf{x}, \mathbf{x}_0) + g_2(\mathbf{x}, \mathbf{x}_0)\right], \quad (1)$$

$$g_i(\mathbf{x}, \mathbf{x}_0) = \frac{iK}{8\pi}\int_{-\infty}^{S_i} \frac{H_1^{(1)}(K\overline{r}_i\sqrt{1+u^2})}{\sqrt{1+u^2}}\,\mathrm{d}u, \quad (2)$$

where $H_n^{(1)}(\cdot)$ is the Hankel function of the first kind, and,

$$\beta = \sqrt{1-M_0^2}, \quad X = \frac{x}{\beta}, \quad K = \frac{\omega}{c}\frac{1}{\beta},$$

$$\overline{r}_{1,2} = \left[(X-X_0)^2 + (y \mp y_0)^2 + (z-z_0)^2\right]^{1/2},$$

$$= \left[\overline{r}^2 + \overline{r}_0^2 - 2\overline{r}\overline{r}_0\cos\left(\overline{\theta} \mp \overline{\theta}_0\right) + (z-z_0)^2\right]^{1/2},$$

$$S_1 = \frac{2\sqrt{\overline{r}\overline{r}_0}}{\overline{r}_1}\cos\frac{\overline{\theta}-\overline{\theta}_0}{2}, \quad S_2 = -\frac{2\sqrt{\overline{r}\overline{r}_0}}{\overline{r}_2}\cos\frac{\overline{\theta}+\overline{\theta}_0}{2},$$

$$\overline{r} = \sqrt{X^2+y^2}, \quad \overline{\theta} = \tan^{-1}\frac{y}{X}.$$

For convenience, we note that the form of (1) is that of calculating the sound from a source and its image in the plane $y = 0$. If we take θ_1 as the coordinate of the source and define $\theta_2 = \theta_1 - 2\pi$ as the coordinate of the image, the acoustic field can be calculated as the sum of the fields g_i from the source and its image, using,

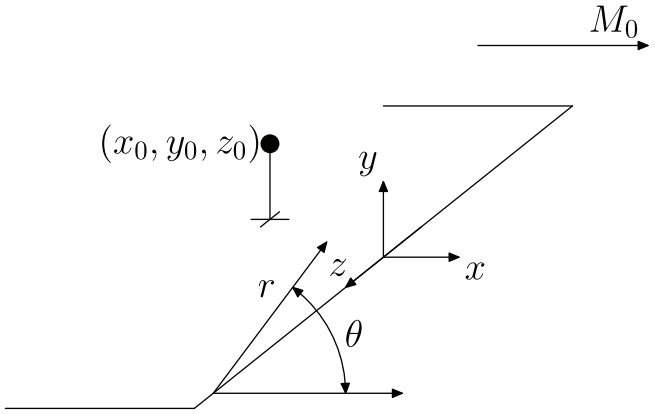

Figure 1. Notation for semi-infinite plate scattering.

$$\overline{r}_i = \left[\overline{r}^2 + \overline{r}_0^2 - 2\overline{r}\overline{r}_0\cos\left(\overline{\theta} - \overline{\theta}_i\right) + (z-z_0)^2\right]^{1/2}, \quad (3)$$

$$S_i = \frac{2\sqrt{\overline{r}\overline{r}_0}}{\overline{r}_i}\cos\frac{\overline{\theta}-\overline{\theta}_i}{2}. \quad (4)$$

We rewrite (2) in a form which facilitates physical interpretation when applied to the rotor noise problem, and can be used to efficiently approximate the field in different regions. Using the result,

$$\int_0^\infty \frac{H_1^{(1)}(K\overline{r}_i\sqrt{1+u^2})}{\sqrt{1+u^2}}\,\mathrm{d}u = -i\frac{e^{iK\overline{r}_i}}{K\overline{r}_i},$$

we can write g_i in a number of alternative forms,

$$g_i(\mathbf{x}, \mathbf{x}_0) = \frac{e^{iK\overline{r}_i}}{4\pi\overline{r}_i} - \frac{iK}{8\pi}\mathcal{L}'(K\overline{r}_i, S_i), \quad (5)$$

$$= \frac{e^{iK\overline{r}_i}}{8\pi\overline{r}_i} + \frac{iK}{8\pi}\mathcal{L}(K\overline{r}_i, S_i), \quad (6)$$

where for convenience, we define the functions,

$$\mathcal{L}(t,s) = \int_0^s \frac{H_1^{(1)}(t\sqrt{1+u^2})}{\sqrt{1+u^2}}\,\mathrm{d}u, \quad (7)$$

$$\mathcal{L}'(t,s) = \int_s^\infty \frac{H_1^{(1)}(t\sqrt{1+u^2})}{\sqrt{1+u^2}}\,\mathrm{d}u. \quad (8)$$

The evaluation of the Green's function for scattering by the plate requires the evaluation of the integrals of (7) and (8). A solution for most of the far field will be found by approximating (8), while an exact expansion for (7) will be developed and used to find a solution for the remaining part of the field.

Integration by parts gives an asymptotic approximation for $\mathcal{L}'(\cdot)$,

$$\int_s^\infty \frac{H_1^{(1)}(t\sqrt{1+u^2})}{\sqrt{1+u^2}}\,\mathrm{d}u \sim \frac{H_0^{(1)}(t\sqrt{1+s^2})}{ts}, \quad t \to \infty, \quad (9)$$

so that for large $K\overline{r}_i$,

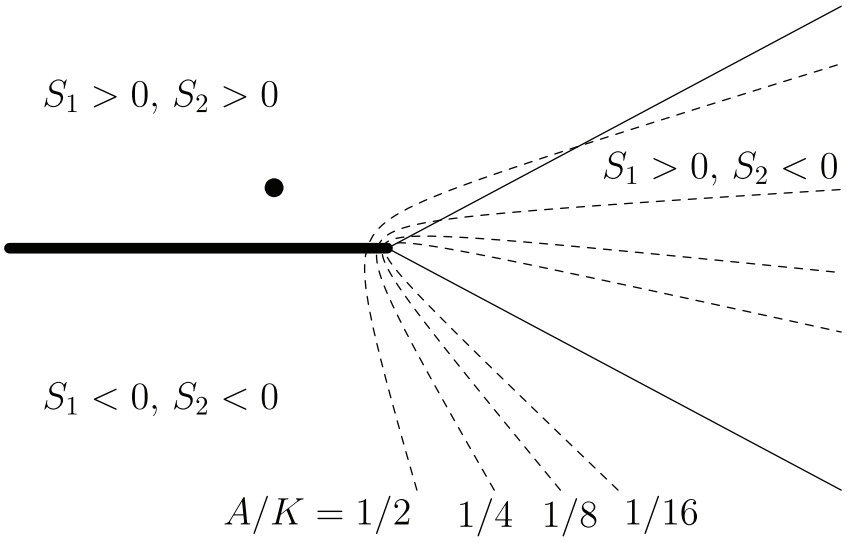

Figure 2. Contribution of acoustic source and image in different regions. Thick line: plate; solid lines: $S_{1,2} = 0$; dashed lines hyperbolae of (11).

$$g_i(\mathbf{x}, \mathbf{x}_0) \approx -i\frac{H_0^{(1)}(Kv)}{8\pi|\bar{r}_i S_i|} + \frac{e^{iK\bar{r}_i}}{4\pi\bar{r}_i} H(S_i), \qquad (10)$$
$$v^2 = (\bar{r} + \bar{r}_0)^2 + (z - z_0)^2,$$

and $H(\cdot)$ is the Heaviside step function.

The asymptotic expression (10) is clearly unbounded for $|S_i| \to 0$ and is invalid in the vicinity of $S_{1,2} = 0$. From the definition of S_i, it is clear that this is the region around the lines through the source and the trailing edge and through the image source and the edge, Figure 2.

Jones [13] discusses the behaviour of the acoustic field in different regions in terms of geometric acoustics. Where $S_i > 0$, the free-field Green's function is "switched on" and the field is that of a source and its reflection in the plane. Where $S_i < 0$, the plate blocks the direct contribution from the source and only the second term of (10) contributes, defining the "shadow" region. Near the boundaries of these two regions, the asymptotic expression breaks down. In the notation of this paper, the asymptotic expression is reasonable outside a region bounded by the hyperbola [13]

$$K(\bar{r} + \bar{r}_0 - \bar{r}_1) = A, \qquad (11)$$

with Jones taking $A = 10$ as a reasonable value. As well as the lines $S_i = 0$, Figure 2 shows the hyperbola of (11) for different values of A/K. The axis of the hyperbolae is $S_i = 0$ and they contract with increasing K. At low frequency the asymptotic approximation breaks down in a large region of the field. As K increases, geometric acoustics is a better approximation and more of the field is well modelled by the asymptotic formula.

In order to find an expansion which can be used for small S_i, we apply the product theorem for Bessel functions ([15], 8.530.2) to (6),

$$\frac{H_1^{(1)}(t\sqrt{1+u^2})}{\sqrt{1+u^2}} = 2\sum_{q=0}^{\infty}(-1)^q(2q+1)H_{2q+1}^{(1)}(t)\frac{J_{2q+1}(tu)}{tu}. \qquad (12)$$

Upon integration of the Bessel functions of the first kind,

$$\mathcal{L}(t,s) = \frac{2}{t}\sum_{q=0}^{\infty}(-1)^q H_{2q+1}^{(1)}(t)\left[J_{2q+1}(ts) + 2\sum_{k=1}^{\infty}J_{2q+2k+1}(ts)\right], \qquad (13)$$

which is exact for $|s| < 1$, though slow to converge as $|s| \to 1$. This result can be used to evaluate the acoustic field in the region $s \to 0$.

2.2 Acoustic field of a ring source near a trailing edge

We now apply the results of Section 2.1 to the estimation of the acoustic field of a rotating source impinging on the edge of a semi-infinite plate. The system is modelled as a ring source and its image in the plane, with the field of each calculated using the "partial" Green's function $G_{1,2}$ with,

$$G_i(\mathbf{x}, \mathbf{x}_0) = \frac{e^{-iKM_0(X - X_0)}}{\beta} g_i(\mathbf{x}, \mathbf{x}_0), \qquad (14)$$

with the principal source denoted by subscript 1 and its image by subscript 2.

As is standard for rotor noise problems [16–20], the source is taken to vary as $\exp[in\psi_0]$ where ψ_0 is the angular variable on a circular source. To respect the image system, the image ring source has azimuthal variation $\exp[-in\psi_0]$ and its field can be calculated using the same analysis, changing n to $-n$.

The ring is centred at a point $(x_0, h, 0)$ with coordinates on the source given by,

$$\mathbf{x}_0 = (x_0, h + a\cos\psi_0,\ a\sin\psi_0),$$

where a is the radius of the source. We introduce spherical coordinates centred on each ring source (Fig. 3),

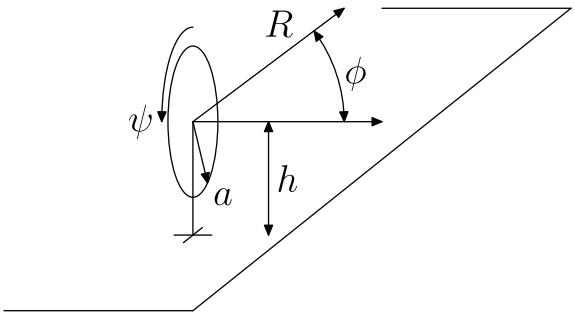

Figure 3. Coordinate system for evaluation of acoustic field of ring source.

$$X - X_0 = R_i \cos\phi_i,$$
$$y \mp h = R_i \sin\phi_i \cos\psi_i,$$
$$z = R_i \sin\phi_i \sin\psi_i.$$

The acoustic field of each source is then given by,

$$p_i(\mathbf{x}) = \frac{e^{-iKM_0(X-X_0)}}{\beta} \int_0^{2\pi} e^{in\psi_0} g_i(\mathbf{x}, \mathbf{x}_0)\, \mathrm{d}\psi_0. \tag{15}$$

We now develop an approximation for p_i valid in the far field.

We treat the field as made up of two contributions, corresponding to the "direct" field generated by the ring source, and that scattered by the trailing edge. The "ring" term is the familiar integral,

$$\mathcal{R}_n(K, a, R_i, \phi_i, \psi_i) = \int_0^{2\pi} \frac{e^{i(K\bar{r}_i + n\psi_0)}}{4\pi\bar{r}_i}\, \mathrm{d}\psi_0, \tag{16}$$

for which a number of exact [20] and approximate [16, 18] expressions exist.

To evaluate the part of the field scattered by the trailing edge, we define the functions,

$$\mathcal{E}_n(K, a, \bar{r}_0, \bar{r}_i, S_i) = \frac{iK}{8\pi} \int_0^{2\pi} e^{in\psi_0} \mathcal{L}(K\bar{r}_i, S_i) \mathrm{d}\psi_0; \tag{17}$$

$$\mathcal{E}'_n(K, a, \bar{r}_0, \bar{r}_i, S_i) = \frac{iK}{8\pi} \int_0^{2\pi} e^{in\psi_0} \mathcal{L}'(K\bar{r}_i, S_i)\, \mathrm{d}\psi_0. \tag{18}$$

In the spherical coordinate system, $\bar{r}_i$ is given by,

$$\bar{r}_i^2 = R_i^2 + a^2 - 2a(y \mp h)\cos\psi_0 - 2az\sin\psi_0,$$
$$= R_i^2 + a^2 - 2R_i a \sin\phi_i \cos(\psi_0 - \psi_i).$$

Differentiating with respect to a and neglecting terms less than $O(1/R_i)$ yields a far-field approximation,

$$\bar{r}_i \approx R_i - a\sin\phi_i \cos(\psi_0 - \psi_i),$$
$$\frac{1}{\bar{r}_i} \approx \frac{1}{R_i},$$

which, upon insertion into (15) and use of tables ([15], 8.411), yields the familiar result for the acoustic field of a ring source ([16–18], among many others),

$$\mathcal{R}_n(K, a, R_i, \phi_i, \psi_i) \approx (-i)^n e^{in\psi_i} \frac{e^{iKR_i}}{2R_i} J_n(Ka\sin\phi_i),$$

where $J_n(\cdot)$ is the Bessel function of the first kind. The free-field part of the ring-source field is then given by,

$$p_i^{(f)}(\mathbf{x}) \approx \frac{e^{-iKM_0(X-X_0)}}{\beta} \mathcal{R}_n(K, a, R_i, \phi_i, \psi_i). \tag{19}$$

We can apply a similar approach to the approximation of the scattered field. Given,

$$v^2 = \bar{r}_1^2(1 + S_1^2) = \bar{r}_2^2(1 + S_2^2) = (\bar{r} + \bar{r}_0)^2 + (z - z_0)^2,$$

to first order in a,

$$v \approx v_0 + \frac{hSa}{v_0}\cos(\psi_0 + \alpha),$$

$$v_0 = \left[\left(\bar{r} + \sqrt{X_0^2 + h^2}\right)^2 + z^2\right]^{1/2},$$

$$\alpha = \tan^{-1}\frac{z/h}{1 + \bar{r}/\sqrt{X_0^2 + h^2}},$$

$$S^2 = \left(\frac{\bar{r}}{\sqrt{X_0^2 + h^2}} + 1\right)^2 + \left(\frac{z}{h}\right)^2.$$

Using Neumann's addition theorem ([21], 10.23),

$$H_0^{(1)}(Kv) \approx H_0^{(1)}\left(Kv_0 + \frac{KhSa}{v_0}\cos(\psi_0 + \alpha)\right),$$
$$= \sum_{q=-\infty}^{\infty} H_q^{(1)}(Kv_0) J_{-q}\left(K\frac{hSa}{v_0}\cos(\psi_0 + \alpha)\right).$$

With the use of tables ([15], 6.681.8, ~9), it is readily shown that for n and q both odd or both even, the integral,

$$\int_0^{2\pi} e^{in\psi} J_q(\alpha\cos\psi)\, \mathrm{d}\psi = 2\pi J_{(q-n)/2}(\alpha/2) J_{(q+n)/2}(\alpha/2), \tag{20}$$

and is identically zero otherwise. This yields,

$$\int_0^{2\pi} H_0^{(1)}(Kv) e^{in\psi_0}\, \mathrm{d}\psi_0 \approx$$

$$2\pi \mathrm{e}^{-in\alpha} \sum_{q=-\infty}^{\infty} H_{2q+\delta}^{(1)}(Kv_0) J_{-(n'+q+\delta)}\left(K\frac{hSa}{2v_0}\right) J_{(n'-q)}\left(K\frac{hSa}{2v_0}\right),$$

where $n = 2n' + \delta$, $\delta = 0, 1$.

The part of the ring-source field scattered by the trailing edge,

$$\mathcal{E}'_n(K, a, \bar{r}_0, \bar{r}_i, S_i) = \frac{iK}{8\pi} \int_0^{2\pi} e^{in\psi_0} \mathcal{L}'(K\bar{r}_i, S_i)\, \mathrm{d}\psi_0,$$

is then approximated by,

$$\mathcal{E}'_n(K,a,\overline{r}_0,\overline{r}_i,S_i) \approx$$

$$-\frac{i}{4}\frac{e^{-in\alpha}}{\sqrt{v_0^2-R_i^2}}\sum_{q=-\infty}^{\infty} H^{(1)}_{2q+\delta}(Kv_0)J_{-(n'+q+\delta)}\left(K\frac{hSa}{2v_0}\right)J_{(n'-q)}\left(K\frac{hSa}{2v_0}\right). \tag{21}$$

This approximation breaks down between the free-field being switched on or off where S_i is small ($v_0 \approx R_i$) and a different approximation is required in this region.

Again, we proceed by approximating for the far field and using the properties of Bessel functions to find a form suitable for evaluation.

Returning to (13),

$$\mathcal{L}(\alpha,s) = \frac{2}{\alpha}\sum_{q=0}^{\infty}(-1)^q H^{(1)}_{2q+1}(\alpha)\left[J_{2q+1}(\alpha s) + 2\sum_{k=1}^{\infty} J_{2q+2k+1}(\alpha s)\right],$$

and noting that $\alpha = K\overline{r}_i$, we seek an approximation which can be inserted into (15) and integrated. In the far field, $K\overline{r}_i \to \infty$, the difficulty lies in capturing the rapid variation in $K\overline{r}_i s_i$ as $s_i \to 0$. We proceed as follows to develop a tractable far-field approximation. The Hankel function is replaced by an approximation valid to first order in a, using the standard relations for derivatives,

$$H_m(K\overline{r}_i) \approx H_m(KR_i) + KaH_{m+1}(KR_i)\sin\phi_i\cos(\psi_0-\psi_i) + O(1/(KR_i)^2).$$

The argument of the Bessel function of the first kind is approximated by,

$$K\overline{r}_i s_i \approx 2K\sqrt{\overline{r}\overline{r}_0}\cos\frac{\overline{\theta}-\overline{\theta}_0}{2} + Ka\sqrt{\frac{\overline{r}}{\overline{r}_0}}\sin\frac{\overline{\theta}+\overline{\theta}_0}{2}\cos\psi_0,$$

and again using the product theorem ([15], 8.530.2),

$$J_m(K\overline{r}_i s_i) \approx \sum_{k=-\infty}^{\infty} J_{m-k}\left(2K\sqrt{\overline{r}\overline{r}_0}\cos\frac{\overline{\theta}-\overline{\theta}_0}{2}\right) \times J_k\left(Ka\sqrt{\frac{\overline{r}}{\overline{r}_0}}\sin\frac{\overline{\theta}+\overline{\theta}_0}{2}\cos\psi_0\right),$$

yielding,

$$\mathcal{L}(K\overline{r}_i,s_i) \approx$$

$$\frac{2}{KR_i}\sum_{q=0}^{\infty}(-1)^q\left[H^{(1)}_{2q+1}(KR_i) + Ka\sin\phi_i H^{(1)}_{2q+2}(KR_i)\cos(\psi_0-\psi_i)\right] \times\left\{\sum_{m=-\infty}^{\infty} J_m(\gamma_2\cos\psi_0)\left[J_{2q+1-m}(\gamma_1) + 2\sum_{k=1}^{\infty} J_{2q+2k+1-m}(\gamma_1)\right]\right\}, \tag{22}$$

$$\gamma_1 = 2K\sqrt{\overline{r}\overline{r}_0}\cos\frac{\overline{\theta}-\overline{\theta}_0}{2}, \quad \gamma_2 = Ka\sqrt{\frac{\overline{r}}{\overline{r}_0}}\sin\frac{\overline{\theta}+\overline{\theta}_0}{2},$$

where all source coordinates such as $\overline{\theta}$ are evaluated at $a = 0$, the centre of the ring. Using (20), for $n = 2n'$,

$$\mathcal{E}_n(K,a,\overline{r}_0,\overline{r}_i,S_i) =$$

$$\frac{iK}{8\pi}\int_0^{2\pi}\mathcal{L}(K\overline{r}_i,s_i)e^{in\psi_0}\,\mathrm{d}\psi_0 \approx$$

$$\frac{\mathrm{i}}{2R_i}\left\{\sum_{q=0}^{\infty}(-1)^q H^{(1)}_{2q+1}(KR_i)\sum_{m=-\infty}^{\infty} J_{m-n'}\left(\frac{\gamma_2}{2}\right)J_{m+n'}\left(\frac{\gamma_2}{2}\right)M_1(\gamma_1) + e^{-i\psi_i}\frac{Ka\sin\phi_i}{2}\sum_{q=0}^{\infty}(-1)^q H^{(1)}_{2q+2}(KR_i) \times\sum_{m=-\infty}^{\infty} J_{m-n'}\left(\frac{\gamma_2}{2}\right)J_{m+n'+1}\left(\frac{\gamma_2}{2}\right)M_2(\gamma_1) + e^{i\psi_i}\frac{Ka\sin\phi_i}{2}\sum_{q=0}^{\infty}(-1)^q H^{(1)}_{2q+2}(KR_i) \times\sum_{m=-\infty}^{\infty} J_{m-n'}\left(\frac{\gamma_2}{2}\right)J_{m+n'-1}\left(\frac{\gamma_2}{2}\right)M_3(\gamma_1)\right\}, \tag{23}$$

where the auxiliary quantities are,

$$M_1(\gamma_1) = J_{2(q-m)+1}(\gamma_1) + 2\sum_{k=1}^{\infty} J_{2(q+k-m)+1}(\gamma_1),$$

$$M_2(\gamma_1) = J_{2(q-m)}(\gamma_1) + 2\sum_{k=1}^{\infty} J_{2(q+k-m)}(\gamma_1),$$

$$M_3(\gamma_1) = J_{2(q-m+1)}(\gamma_1) + 2\sum_{k=1}^{\infty} J_{2(q+k-m+1)}(\gamma_1).$$

2.3 Summary

To summarize, the far-field sound from a rotor near the edge of a semi-infinite plane can be estimated by summing the contribution from the circular source of azimuthal order n and from its image in the plane, of order $-n$. For each source, the acoustic field is estimated by first determining the appropriate far-field approximation to apply. Figure 4 shows the region around a rotor divided according to the sign of S_i, with the hyperbolae of (11) added for source positions at the top and bottom of the rotor, with $A = 10$ and $K = 12/\sqrt{1-0.15^2}$, which corresponds to the sample calculations presented in Section 3. In region I, $S_i > 0$ for all source positions on the rotor while in region II, $S_i < 0$. In region III, S_i changes sign for some value of ψ_0. The appropriate far-field approximation to use in each region is then:

$$p_n = \frac{e^{-iKM_0(X-X_0)}}{\beta}\left(\mathcal{R}_n - \mathcal{E}'_n\right), \quad \text{(I)} \tag{24}$$

$$= -\frac{e^{-iKM_0(X-X_0)}}{\beta}\mathcal{E}'_n, \quad \text{(II)} \tag{25}$$

$$= \frac{e^{-iKM_0(X-X_0)}}{\beta}\left(\frac{\mathcal{R}_n}{2} + \mathcal{E}_n\right), \quad \text{(III)}. \tag{26}$$

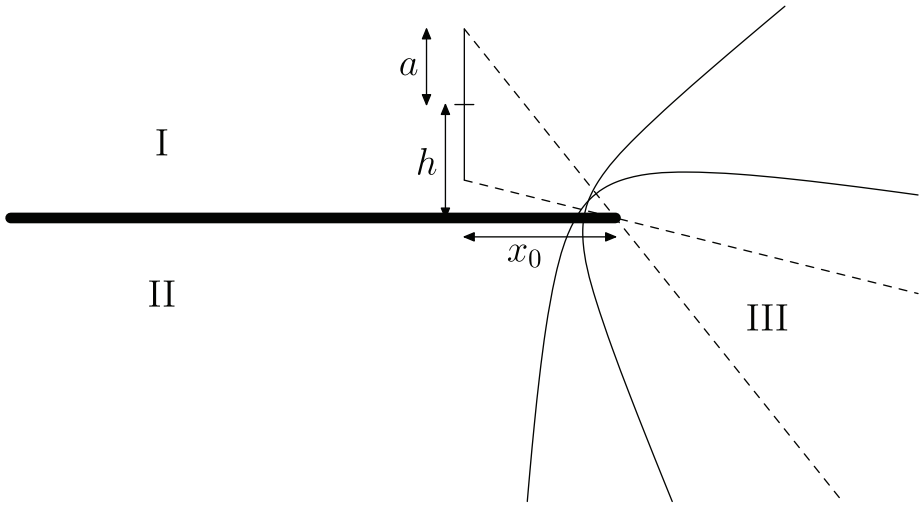

Figure 4. Regions around rotor labelled by far-field approximation. The hyperbolae of (11) are shown for the top and bottom of the rotor with $A = 10$ and $K = 12/\sqrt{1-0.15^2}$.

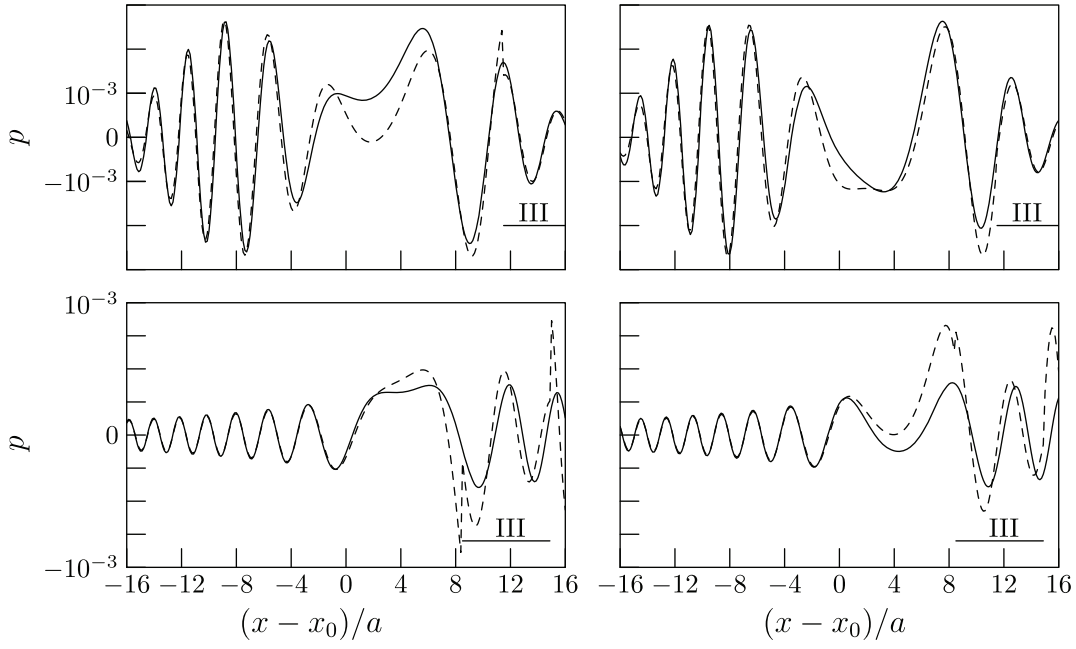

Figure 5. Acoustic potential above and below source; left-hand column: real part; right-hand column: imaginary part; solid line: numerical; dashed line: approximation. Top row: field above source and plate; bottom row: field below source and plate.

In the far field, the functions $\mathcal{R}(\cdot)$, $\mathcal{E}(\cdot)$, and $\mathcal{E}'(\cdot)$ can be evaluated using the results given earlier. Finally, with regard to evaluation of the series defining these functions, we note that the Bessel function of the first kind $J_n(x)$ decays exponentially with increasing order for $n > x$, allowing the series to be truncated with negligible loss of accuracy.

3 Results

To illustrate the application of the method, we present sample results for an arbitrarily selected configuration, with rotor parameters $a = 0.3$, $n = 6$. The rotor is positioned above the plate at $h = 0.9$, and one rotor diameter upstream of the trailing edge at $x_0 = -2a$. The rotor tip Mach number M_t is set to 0.6, so that the wavenumber $k = nM_t/a = 12$, and the flow Mach number $M_0 = 0.15$. The acoustic field is evaluated using the methods of this paper, and compared to full numerical evaluation, with results calculated above and below the plate to examine the shielding effect.

Figure 5 shows the real and imaginary part of the potential at $-16a \le x - x_0 \le 16a$, $z = 0$, i.e. directly above and below the source centre. Results are calculated at a constant vertical displacement above and below the

source, $y = h \pm 16a$. The two upper plots show the acoustic potential above the source and the plate, and the lower plots show the field below the plate, at the same distance from the source as in the upper plots. The region marked "III" on each plot shows where (26) has been applied, in the transition region where the asymptotic approximation for the edge-scattered field breaks down. The beginning of this breakdown is apparent at the end of region III, in particular in the lower left-hand plot of the figure, where the difference between the asymptotic approximation and the numerical evaluation is clear for $(x - x_0)/a \gtrapprox 0$. This corresponds to the hyperbolic boundary shown in Figure 4, which has been drawn for the same value of K as used in the calculations.

In applications, where the rotor may be placed above a wing in order to benefit from shielding effects, the region of interest is the "shadow zone" upstream of the trailing edge. The upper and lower fields are computed at constant distance from the source, so the different scales on the upper and lower plots make the shielding effect clear. In this case, the maximum amplitude upstream of the trailing edge is about ten times greater above the plate than below, and is well predicted by the far field approximation.

We note that while the results presented demonstrate good accuracy, the analysis is limited by the assumptions made in its development. In particular, the analysis does assume small source radius a and numerical experimentation has found that the accuracy of predictions degrades as a is increased. This may limit the applicability of the method, in particular as a becomes comparable to h, the case of a rotor with a small tip clearance above the wing, or where the rotor lies close to the trailing edge.

4 Conclusions

An approximate analysis has been developed for the radiation of sound from a rotating source near the edge of a semi-infinite plate in a uniform flow, a model problem for shielding and scattering of rotor noise by a wing. Sample calculations for small source radius show good agreement with full numerical evaluation, and capture the wing shielding effect reasonably accurately. Future work will focus on improving the accuracy and range of validity of the approximation, in particular in the case of small clearance between the rotor and wing. An open question is that of whether there is a useful exact expansion for the acoustic field, comparable to the series solutions which exist for isolated rotors.

Conflict of interest

The author declares that he has no conflicts of interest in relation to this article.

Acknowledgments

The author is indebted to the anonymous reviewer who brought the paper of Jones [13] to his attention.

References

1. A. Agarwal, A.P. Dowling: Low-frequency acoustic shielding by the Silent Aircraft airframe. AIAA Journal 45, 2 (2007) 358–365.
2. P. Eret, J. Kennedy, F. Amoroso, P. Castellini, G.J. Bennett: Experimental observations of an installed-on-pylon contra-rotating open rotor with equal blade number in pusher and tractor configuration. International Journal of Aeroacoustics 15, 1–2 (2016) 228–249.
3. M. Czech, R.H. Thomas: Open rotor installed aeroacoustic testing with conventional and unconventional airframes, in: 19th AIAA/CEAS Aeroacoustics Conference, Berlin, Germany, May 27–29, 2013.
4. C.J. Bahr, R.H. Thomas, L.V. Lopes, C.L. Burley, D.E. Van Zante: Open rotor tone shielding methods for system noise assessments using multiple databases, in: 52nd AIAA Aerospace Sciences Meeting, National Harbor, Maryland, 13–17 January, 2014. AIAA.
5. Y. Guo, M.J. Czech, R.H. Thomas, Open rotor noise shielding by blended-wing-body aircraft, in: 19th AIAA/CEAS Aeroacoustics Conference, Berlin, Germany, May 27–29, 2013.
6. Y. Guo, R.H. Thomas: Experimental study on open rotor noise shielding by Hybrid-Wing-Body aircraft. AIAA Journal 54, 1 (2016) 242–253.
7. L. Dürrwächter, M. Keßler, E. Krämer: Numerical assessment of open-rotor noise shielding with a coupled approach. AIAA Journal 57, 5 (May 2019) 1930–1940.
8. M. Lummer, C. Richter, C. Pröber, J. Delfs: Validation of a model for open rotor noise predictions and calculation of shielding effects using a fast BEM, in: 19th AIAA/CEAS Aeroacoustics Conference, Berlin, Germany, May 27–29, 2013.
9. M. Lummer, M. Mößner, J.W. Delfs: Computation and validation of acoustic shielding at realistic aircraft configurations, in: 2018 AIAA/CEAS Aeroacoustics Conference, Atlanta, Georgia, June 25–29, 2018.
10. D.B. Stephens, E. Envia, Acoustic shielding for a model scale counter-rotation open rotor, 17th AIAA/CEAS Aeroacoustics Conference (32nd AIAA Aeroacoustics Conference), Portland, Oregon, 05–08 June, 2011.
11. K.M. Li, H.Y. Wong: A review of commonly used analytical and empirical formulae for predicting sound diffracted by a thin screen. Applied Acoustics 66, 1 (2005) 45–76.
12. H.M. Macdonald: A class of diffraction problems. Proceedings of the London Mathematical Society s2_14, 1 (1915) 410–427.
13. D.S. Jones: The mathematical theory of noise shielding. Progress in Aerospace Sciences 17 (1977) 149–229.
14. M. Roger, S. Moreau, K. Kucukcoskun: On sound scattering by rigid edges and wedges in a flow, with applications to high-lift device aeroacoustics. Journal of Sound and Vibration 362 (2016) 252–275.
15. I. Gradshteyn, I.M. Ryzhik: Table of integrals, series, and products, 5th ed. Academic, London, 1980.
16. L. Gutin: On the sound field of a rotating propeller. Technical Memorandum 1195, NACA, Langley Aeronautical Laboratory, Langley Field, VA. USA, 1948.
17. I.E. Garrick, C.E. Watkins: A theoretical study of the effect of forward speed on the free-space sound-pressure field around propellers. Report 1198, National Advisory Committee for Aeronautics (NACA). 1953.
18. S.E. Wright: Sound radiation from a lifting rotor generated by asymmetric disk loading. Journal of Sound and Vibration 9, 2 (1969) 223–240.
19. M. Carley: Series expansion for the sound field of rotating sources. Journal of the Acoustical Society of America 120, 3 (September 2006) 1252–1256.

20. M. Carley: Series expansion for the sound field of a ring source. Journal of the Acoustical Society of America 128, 6 (2010) 3375–3380.

21. National Institute of Standards and Technology: Digital library of mathematical functions. 2010. http://dlmf.nist.gov/.

Cite this article as: Carley M. 2022. Shielding of rotor noise by plates and wings. Acta Acustica, **6**, 27.